Proceedings of the 45th IEEE Conference on Decision & Control
Manchester Grand Hyatt Hotel
San Diego, CA, USA, December 13-15, 2006

Variable Control Design and its Application to Wafer Scanners

Marcel Heertjes
Philips Applied Technologies
High Tech Campus 7, room 1A-031-5
5656 AE Eindhoven, The Netherlands
Email address: marcel.heertjes@philips.com

Nathan van de Wouw
Eindhoven University of Technology
Department of Mechanical Engineering
5600 MB Eindhoven, The Netherlands
Email address: n.v.d.wouw@tue.nl

***Abstract*— A variable control design is presented. The validity of such a design in dealing with linear performance trade-offs is demonstrated on a reticle stage motion system of an industrial wafer scanner. Performance is achieved by continuously balancing stability margins over disturbance rejection properties. This is done by a nonlinear state-dependent element in the feedback loop. Apart from performance, design rules and conditions to guarantee stability of the nonlinear system are considered.**

Keywords: Lurie-Postnikov form, Lyapunov stability, nonlinear control, variable gains, stability margins.

I. Introduction

Over the past decades linear feedback control has greatly evolved from a PID-trick [11] to a well-established design philosophy. This includes the means to analyze (and quantify) stability and performance which, combined, provide a great understanding of the design and its design limitations. Inherent limitations such as "waterbed" effects are widely known, see [3], [4]. However effective means to deal with such limitations in the sense of avoiding or balancing them in a more desired manner remain fairly limited.

In this respect, a variable control design may contribute to the control design freedom otherwise encountered having such limitations (see also [7], [8] with a similar purpose but applied to optical storage drives). On the basis of two linear controller limits – one designed with sufficient stability margins and the other designed to achieve improved low-frequency disturbance rejection but at the cost of these margins – nonlinear control is presented as a weighted (state-dependent) sum of both controller limit contributions. For the servo error signals at hand such weighting is achieved by a variable gain function. In an example of a reticle stage motion system of an industrial wafer scanner, a variable control design is demonstrated to achieve improved performance. That is, for a saturation-based gain function, desired stability margins (and subsequent low sensitivities to high-frequency oscillations) are obtained largely under "low-gain" feedback. This typically applies to those parts of a set-point profile that induce high-frequency oscillations. Contrary, improved low-frequency disturbance rejection is obtained under "high-gain" feedback at the remaining parts of the set-point profile, in particular those parts aimed at achieving performance.

This paper is organized in the following manner. First, a general setting for the considered class of nonlinear control systems is provided in Lurie-Postnikov form. Second, frequency-domain stability properties are derived given a class of nonlinearities. Third, an example is given of a variable PID controlled motion system in industrial practice. Fourth, a brief summary of the main conclusions is provided.

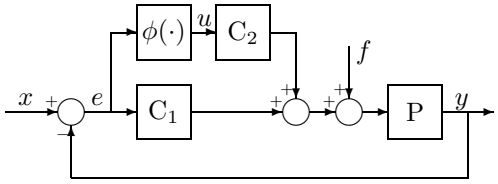

Fig. 1. Nonlinear controlled dynamics in block diagram representation.

II. Variable Controlled Systems

Variable controlled systems such as considered in this paper belong to the class of nonlinear PID controlled systems, see [1] and [2] for a general overview in this field. Such systems can be represented by the block diagram representation of Figure 1. Based on a linear time-invariant PID-based controller C_1, the plant P is controlled such that its output $y \in \mathbb{R}$ tracks the input $x \in \mathbb{R}$ in face of disturbances contained in $f \in \mathbb{R}$ or in x itself. The tracking ability is expressed by the servo error signal $e{=}x - y$. Note that f may contain feedforward control contributions needed to obtain a proper time-domain behavior. In addition to the linear forward path from e to y a nonlinear path is added given by the series connection of a memoryless input-dependent nonlinearity $\phi(\cdot)$ satisfying $0 \leq \phi(\cdot) \leq 1$ and a linear time-invariant controller C_2. The output of the nonlinearity reads $u{=}\ \phi(e)\ e$ with $e \in \mathbb{R}$. The overall nonlinear controller $C_3{=}C_3\ (e)$ is then given by

$$C_3\ (e) = C_1 + C_2\ \phi(e). \tag{1}$$

In this form, the nonlinear controlled dynamics allows for a loop transformation in which a linear time-invariant system in the forward path is separated from a memoryless nonlinearity in the feedback path. Such a Lurie-Postnikov form [10] is depicted in Figure 2.

Proposition II.1 *Assume the feedback connection in Figure 1 with finite continuous inputs $x{=}x\,(t) \in \mathbb{R}$ and $f{=}f\ (t) \in \mathbb{R}$, the linear time-invariant systems C_1, C_2, and P, a memoryless continuous function $\phi(\cdot) \in \mathbb{R}$, and continuous*

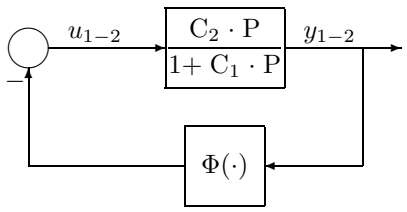

Fig. 2. Nonlinear controlled dynamics in Lurie-Postnikov form.

output $y = y(t) \in \mathbb{R}$. If e, u, and y are unique solutions, then a Lurie-Postnikov form exists as given in Figure 2.

Proof: The existence and uniqueness of the piecewise continuous output $y_{1-2}{=}y_1 - y_2$ and input $u_{1-2}{=}u_1 - u_2$ follows from the existence and uniqueness of the pairs $y_1{\in}\ \mathbb{R}, u_1{\in}\ \mathbb{R}$ and $y_2{\in}\ \mathbb{R}, u_2{\in}\ \mathbb{R}$ both of which merely differ in terms of initial conditions at time $t = t_0$. Using the relations given in Figure 1, it follows that

$$\begin{aligned}\mathcal{L}\{y_1\} = {} & \mathrm{C}_2\ (s)\ \mathrm{P}\ (s) \cdot \mathcal{L}\{u_1\} \\ & + \mathrm{P}\ (s) \cdot \mathcal{L}\{f\ (t)\} + \mathrm{C}_1\ (s)\ \mathrm{P}\ (s) \cdot \mathcal{L}\{e_1\},\end{aligned} \tag{2}$$

with $\mathcal{L}\{\cdot\}$ the Laplace transform of the given signal and s the Laplace variable. Similarly,

$$\begin{aligned}\mathcal{L}\{y_2\} = {} & \mathrm{C}_2\ (s)\ \mathrm{P}\ (s) \cdot \mathcal{L}\{u_2\} \\ & + \mathrm{P}\ (s) \cdot \mathcal{L}\{f\ (t)\} + \mathrm{C}_1\ (s)\ \mathrm{P}\ (s) \cdot \mathcal{L}\{e_2\}.\end{aligned} \tag{3}$$

Subtracting (3) from (2) gives

$$\frac{\mathcal{L}\{y_{1-2}\}}{\mathcal{L}\{u_{1-2}\}} = \frac{\mathrm{C}_2\ (s)\ \mathrm{P}\ (s)}{1+ \mathrm{C}_1\ (s)\ \mathrm{P}\ (s)}, \tag{4}$$

hence the forward path in Figure 2. The feedback path follows from the fact that

$$\begin{aligned} u_{1-2} &= u_1 - u_2 \\ &= \ \phi(e_1)\ e_1 - \phi(e_2)\ e_2 \\ &= -\Phi(e_1, e_2)\ y_{1-2} \end{aligned} \tag{5}$$

with

$$\Phi(e_1, e_2) = -\frac{\phi(e_1)\ e_1 - \phi(e_2)\ e_2}{y_{1-2}}. \tag{6}$$

■

In Lurie-Postnikov form, stability of the nonlinear feedback connection can now be studied given the choice of the variable gain function ϕ, and the filters C_1 and C_2.

III. Variable Gain Functions

The choice for a variable gain function is key to both the stability and the performance of the resulting nonlinear feedback connection. To illustrate this, the following example is considered:

Example III.1 *On the basis of a saturation characteristic, a variable gain is defined as*

$$\phi(y) = \begin{cases} 1, \ \textit{if} \mid y \mid \leq \delta, \\ \dfrac{\delta}{\mid y \mid}, \ \textit{if} \mid y \mid > \delta, \end{cases} \tag{7}$$

with $\phi(\cdot) \in \mathbb{R}$ a continuous function, $y{\in}\ \mathbb{R}$ a continuous input, and $\delta > 0$ a constant. For $|y| \leq \delta$ the output of Eq. (7) equals y. For $|y| > \delta$ a non-proportionally scaled fraction results.

To guarantee stability the choice for variable gain functions ϕ is often restricted (see, e.g, [9], [14], [15] regarding absolute stability). On the one hand by requiring ϕ to be a memoryless function, *i.e.*, it has a static input-output relation, and on the other hand by confining ϕ to a sector $[\delta_1, \delta_2]$ with $\delta_1,\ \delta_2 \in \mathbb{R}$. In the example, not only $\phi(\cdot)$ is confined to the sector $[0, 1]$, *i.e.*, $0 \leq \phi(y) \leq 1$, but also its incremental form,

$$\Phi(y_1, y_2) = \frac{\phi(y_1)\ y_1 - \phi(y_2)\ y_2}{y_1 - y_2}, \tag{8}$$

is confined to this sector, see [5] for a further discussion into incremental stability.

IV. Variable Controller Design

Given a choice for the variable gain function $\phi(\cdot)$ the nonlinear control design further amounts to designing the limit controllers that satisfy the desired performance specifications. For the variable controller structure in Eq. (1) this amounts to designing both C_1 and C_2. The choice for both controllers is limited by the stability properties of the corresponding closed-loop systems. For a given choice of C_1 and C_2 stability can be checked using the next result.

Theorem IV.1 *Assume the strictly proper system* P *that is globally asymptotically stabilized – under uniformly bounded disturbances x and f – either by* C_1 *or by* $\mathrm{C}_2 + \mathrm{C}_1$ *both of which are strictly proper and Hurwitz. Then any controller of the form* $\mathrm{C}_3\ (y) = \mathrm{C}_1 + \mathrm{C}_2\ \phi(y)$ *with* $\phi(\cdot)$ *and its incremental form* $\Phi(\cdot)$ *both memoryless and confined to the sector* $[0, 1]$ *globally asymptotically stabilizes* P *in a bounded-input bounded-output sense if*

$$\Re\left\{\mathrm{G}\ (j\omega) = \frac{\mathrm{C}_2\ (j\omega)\ \mathrm{P}\ (j\omega)}{1+ \mathrm{C}_1\ (j\omega)\ \mathrm{P}\ (j\omega)}\right\} \geq -1. \tag{9}$$

Proof: Since C_1, C_2, and P are strictly proper functions, G is also strictly proper and allows for a state-space realization of the form

$$\begin{aligned} \dot{\mathbf{x}} &= \mathbf{A}\mathbf{x} + \mathbf{b}u_{1-2} \\ y_{1-2} &= \mathbf{c}^{\mathrm{T}}\mathbf{x}, \end{aligned} \tag{10}$$

$\mathbf{x} \in \mathbb{R}^{n\times 1}$, $\mathbf{A} \in \mathbb{R}^{n\times n}$, $\mathbf{b} \in \mathbb{R}^{n\times 1}$, $\mathbf{c} \in \mathbb{R}^{n\times 1}$, which in the Laplace domain is given by the transfer function

$$\frac{y_{1-2}}{u_{1-2}}(s) = \mathbf{c}^{\mathrm{T}}\ (s\ \mathbf{I} - \mathbf{A})^{-1}\ \mathbf{b}\ . \tag{11}$$

Moreover because C_1 (and similarly C_2) globally asymptotically stabilizes P, the closed-loop transfer $\mathrm{P}\ /(1+ \mathrm{C}_1\mathrm{P})$ is Hurwitz which combined with C_2 being Hurwitz gives a G in (9), hence a system matrix $\mathbf{A}$ in (10), that is Hurwitz. Since the pair $(\mathbf{A}, \mathbf{b})$ is controllable and the pair $(\mathbf{A}, \mathbf{c})$ is observable, the Kalman-Yakubovich-Popov theorem, see also [6], [13] and the references therein, guarantees the

existence of a positive definite matrix $\mathbf{P}= \mathbf{P}^{\mathrm{T}} \in \mathbb{R}^{n\times n}$, matrix $\mathbf{q} \in \mathbb{R}^{1\times n}$, and a positive constant $\epsilon > 0$ satisfying

$$\begin{aligned} \mathbf{P}\mathbf{A} + \mathbf{A}^{\mathrm{T}}\mathbf{P} &= -\mathbf{q}^{\mathrm{T}}\mathbf{q} - \epsilon\,\mathbf{P} \\ \mathbf{P}\mathbf{b} &= \mathbf{c} - \sqrt{2}\,\mathbf{q}^{\mathrm{T}}, \end{aligned} \tag{12}$$

for $\mathrm{G}\,(j\omega)$ satisfying (9). On the basis of $\mathbf{P}$, the following Lyapunov function candidate is constructed

$$\mathrm{V}\,(\mathbf{x}) = \mathbf{x}^{\mathrm{T}}\mathbf{P}\mathbf{x}, \tag{13}$$

which is positive definite and whose derivative is given by

$$\begin{aligned} \dot{\mathrm{V}}(\mathbf{x}) &= \mathbf{x}^{\mathrm{T}}\left(\mathbf{A}^{\mathrm{T}}\mathbf{P} + \mathbf{P}\mathbf{A}\right)\mathbf{x} + 2\,u_{1-2}\mathbf{b}^{\mathrm{T}}\mathbf{P}\mathbf{x} \\ &= -\mathbf{x}^{\mathrm{T}}\mathbf{q}^{\mathrm{T}}\mathbf{q}\mathbf{x} - \epsilon\,\mathbf{x}^{\mathrm{T}}\mathbf{P}\mathbf{x} + 2\,u_{1-2}y_{1-2} \\ &\quad - 2\sqrt{2}\,u_{1-2}\mathbf{q}\mathbf{x}\,. \end{aligned} \tag{14}$$

Because $\Phi(\cdot)$ is memoryless and confined to the sector $[0, 1]$, it follows that $u_{1-2}y_{1-2} \leq -\,{u_{1-2}}^2$ such that

$$\begin{aligned} \dot{\mathrm{V}}(\mathbf{x}) &\leq -\mathbf{x}^{\mathrm{T}}\cdot\mathbf{q}^{\mathrm{T}}\cdot\mathbf{q}\cdot\mathbf{x} - \epsilon\,\mathbf{x}^{\mathrm{T}}\cdot\mathbf{P}\cdot\mathbf{x} + 2\,{u_{1-2}}^2 \\ &\quad - 2\sqrt{2}\,u_{1-2}\mathbf{q}\cdot\mathbf{x} \\ &\leq -\epsilon\,\mathbf{x}^{\mathrm{T}}\cdot\mathbf{P}\cdot\mathbf{x} - \left(\mathbf{x}^{\mathrm{T}}\cdot\mathbf{q}^{\mathrm{T}} + \sqrt{2}\,u_{1-2}\right)^2 \\ &\leq -\epsilon\,\mathbf{x}^{\mathrm{T}}\cdot\mathbf{P}\cdot\mathbf{x}, \end{aligned} \tag{15}$$

which is negative definite. Hence the equilibrium point $y_{1-2}= y_1 - y_2= 0$ is globally asymptotically stable. By itself this is not sufficient to prove the theorem because the underlying solutions y_1 and y_2 may escape to infinity while y_{1-2} tends to zero. Given the conditions, however, the feedback connection in Figure 1 can be written as

$$\begin{aligned} \dot{\mathbf{x}} &= \mathbf{A}\cdot\mathbf{x} + \mathbf{b}\,u \\ y &= \mathbf{c}^{\mathrm{T}}\cdot\mathbf{x} - v, \end{aligned} \tag{16}$$

with

$$\mathcal{L}\{v(t)\} = \frac{\{\mathcal{L}\{x(t)\} - \mathrm{P}\;\mathcal{L}\{f(t)\}\}}{1 + \mathrm{C}_1\,(s)\;\mathrm{P}\,(s)}. \tag{17}$$

That is for the non-perturbed system with $v(t) = 0$ the proof repeats itself. For the perturbed system where

$$\rho_{\min}\mathbf{x}^{\mathrm{T}}\cdot\mathbf{x} \leq \mathbf{x}^{\mathrm{T}}\cdot\mathbf{P}\cdot\mathbf{x} \leq \rho_{\max}\mathbf{x}^{\mathrm{T}}\cdot\mathbf{x}, \tag{18}$$

with $\rho_{\min}$ and $\rho_{\max}$ the minimal and maximal singular values of $\mathbf{P}$ respectively, it follows that

$$\dot{\mathrm{V}}(\mathbf{x}) \leq -\|\,\mathbf{x}\,\|_{\mathrm{p}}\left\{\epsilon\|\,\mathbf{x}\,\|_{\mathrm{p}} - 2\,\mathrm{c}_1\,\|\,\mathbf{b}\,\|_{\mathrm{p}}\right\}, \tag{19}$$

with c_1 a uniform bound on v, $\|\,\mathbf{x}\,\|_{\mathrm{p}} = \sqrt{\mathbf{x}^{\mathrm{T}}\mathbf{P}\mathbf{x}}$ a p-norm on $\mathbf{x}$, and $\|\,\mathbf{b}\,\|_{\mathrm{p}} = \sqrt{\mathbf{b}^{\mathrm{T}}\mathbf{P}\mathbf{b}}$ a p-norm on $\mathbf{b}$. This leaves

$$\varepsilon = \left\{\mathbf{x}\in\mathbb{R}^n,\ \|\,\mathbf{x}\,\|_{\mathrm{p}} \geq \frac{2\,\mathrm{c}_1\,\|\,\mathbf{b}\,\|_{\mathrm{p}}}{\epsilon}\right\}, \tag{20}$$

a positively invariant set to which all solutions converge. ■

Remark IV.2 *From a stability standpoint, Theorem IV.1 can be used as a design tool for tuning* C_2*. Suppose that (9) is not satisfied which given the properties of* C_1*,* C_2*, and* P *occurs on the domain* $\omega \in (0, \infty)$*. Then evaluation of the closed-loop characteristics of* $\mathrm{C}_2\mathrm{P}\,/(1+\,\mathrm{C}_1\mathrm{P})$ *at those frequency regions where (9) is violated, ideally gives the loop shaping characteristics of* C_2 *needed to avoid such a violation. As a result an updated* C_2 *can be constructed that incorporates such characteristics in some approximative sense.*

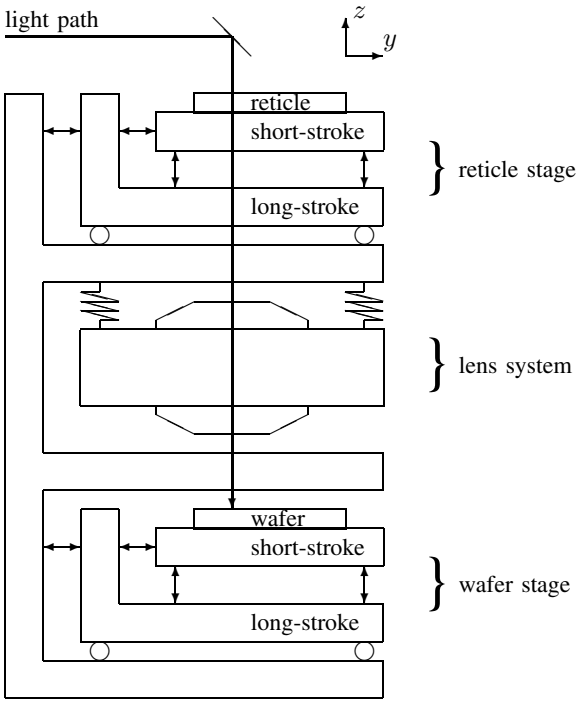

Fig. 3. Schematic representation of a wafer scanner.

Having derived sufficient conditions to check for stability let us now consider some of the possibilities a variable gain design may have in terms of performance improvement of the reticle stage motion system of an industrial wafer scanner.

V. Variable PID-based Control with Applications to a Wafer Scanner

In the manufacturing of integrated circuits (IC), wafer scanners provide the means to achieve both position accuracy and production speed. Scanners typically achieve 70 nanometer resolution with a throughput of hundred wafers an hour each wafer containing over hundred ICs, see, for example, [12] for a detailed specification on nowadays available scanners based on immersion lithography.

A schematic representation of a wafer scanner is shown in Figure 3. Light from a laser passes a reticle – a quartz object containing the image – through a lens, which scales down the desired image by a factor of four, and onto a wafer. The latter is represented by a silicon disk. Both reticle and wafer are part of two separate motion controlled sub-systems: the reticle stage and the wafer stage, respectively, each employing a dual-stroke strategy. A long-stroke stage is used for fast (large-range) motion whereas a short-stroke stage is used for accurate (small-range) tracking. The short-stroke stages are represented by floating masses which are controlled on a single-input single-output basis in six degrees-of-freedom.

In scanning (y) direction, see Figure 3, the reticle stage performs repetitive tasks along a pre-defined set-point pro-

file. Herein two regions can be distinguished: first, a non-stationary region where the system accelerates and is exposed to large levels of excitation and second, a stationary region where the system moves at constant velocity (scanning) and is expected to achieve performance. To improve upon the disturbance rejection properties during the stationary region, but not to deteriorate the stability properties in the non-stationary region where large control forces challenge the linear model assumptions, a variable PID-based controller is demonstrated to achieve improved performance.

A. Saturation-based variable gain

Based on a saturation characteristic, see the right part of Figure 4, a variable gain function $\phi(e)$ is chosen according to Eq. (7). In terms of variable gains, see the left part of this figure, the input signals e inside the bounds defined by

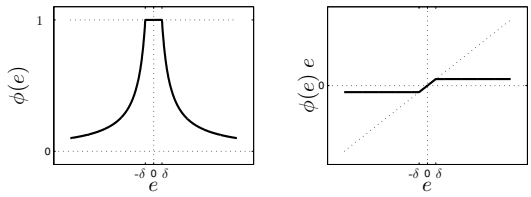

Fig. 4. Saturation-based variable gain characteristics.

the saturation length δ are passed through unscaled. Outside these bounds, the output becomes a non-proportionally scaled fraction of the input where $\phi(e) \to 0$ for $\mid e \mid \to \infty$.

B. PID-based controller limits

The controllers C_1 and C_2, see also Eq. (1), are proportional-integrator-derivative (PID)-based controllers with additional filters designed according to loop-shaping arguments. In discrete-time, they are represented by

$$\begin{aligned}\mathrm{C}_1\ (z) =& \frac{2.93\cdot 10^8 z^8 - 3.89\cdot 10^8 z^7 - 2.62\cdot 10^7 z^6}{z^9 - 1.78 z^8 + 2.36 z^7 - 2.36 z^6} \cdots \\ \cdots & \frac{+3.64\cdot 10^8 z^5 - 4.30\cdot 10^8 z^4 + 3.64\cdot 10^8 z^3}{+1.61 z^5 - 0.63 z^4 + 0.03 z^3} \cdots \\ \cdots & \frac{-3.10\cdot 10^7 z^2 - 3.47\cdot 10^8 z^1 + 2.20\cdot 10^8}{+0.03 z^2 - 0.20 z - 0.05},\end{aligned} \tag{21}$$

and

$$\mathrm{C}_2\ (z) = \frac{\alpha(0.08 z^3 - 0.02 z^2 - 0.06 z + 0.04)}{z^4 - 1.46 z^3 + 0.67 z^2 - 0.16 z + 4.1\cdot 10^{-4}} \cdot \mathrm{C}_1\ (z), \tag{22}$$

with $z \in \mathbb{C}$ the z-domain operator and $\alpha = 2.5$. This gives two linear controller limits:

1) $\mathrm{C}_1\ (z)$ if $\phi(y) = 0$, $\forall\ y \in \mathbb{R}$,
2) $\mathrm{C}_1\ (z) + \mathrm{C}_2\ (z)$ if $\phi(y) = 1$, $\forall\ y \in \mathbb{R}$.

Both controller limits are depicted in Bode representation in Figure 5. Herein, the low-frequency difference between C_1 and C_2 is caused by the gain difference of $1 + \alpha = 3.5$.

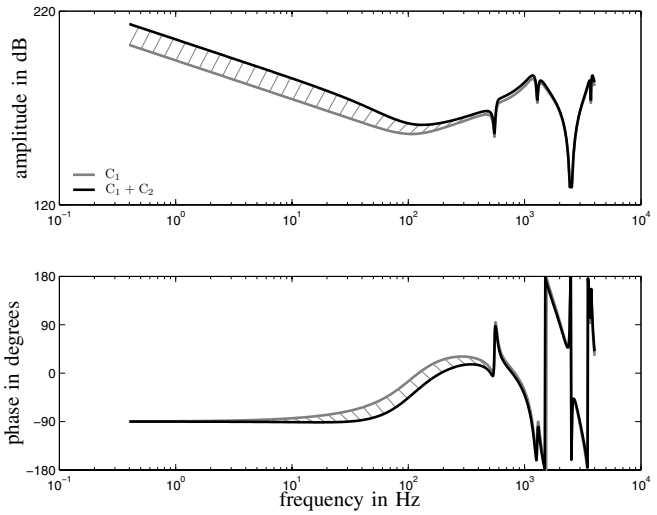

Fig. 5. Controller limits $\mathrm{C}_1\ (j\omega)$ and $\mathrm{C}_2\ (j\omega)$ in Bode representation.

C. Frequency-domain stability analysis

Stability of the nonlinear feedback connection can be checked with Eq. (9). For this purpose, a graphical interpretation is derived such as given in the left part of Figure 6. Here stability is sufficiently guaranteed if $G(j\omega)$ in Nyquist

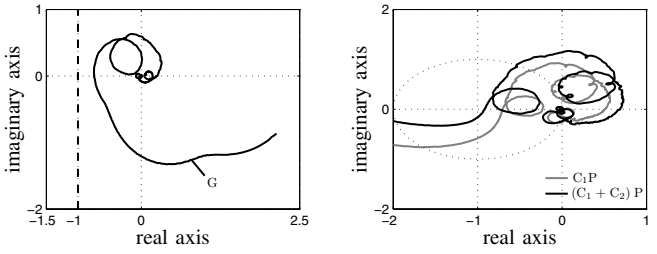

Fig. 6. a) closed-loop frequency response function G $(j\omega)$, and b) open-loop frequency response functions $\mathrm{C}_1\ (j\omega)$ P $(j\omega)$ and $(\mathrm{C}_1\ (j\omega) + \mathrm{C}_2\ (j\omega))$ P $(j\omega)$ in Nyquist representation.

representation remains to the right of a vertical line through the point (-1,0). Clearly this is satisfied for the frequency response function $G(j\omega)$ measured on a real wafer scanner where some stability margin is taken into account. In the right part of Figure 6, the measured open-loop frequency response functions based on the two linear controller limits C_1 and $\mathrm{C}_1 + \mathrm{C}_2$ are depicted. It follows that the control design based on C_1 corresponds to a phase margin of 28 degrees (and a gain margin of -3 dB) versus a phase margin of 8 degrees (and a gain margin of -0.74 dB) for the control design based on $\mathrm{C}_1 + \mathrm{C}_2$, hence the latter induces much tighter stability margins.

D. Time-domain performance

For the considered nonlinear control design, measured time-series of the servo error signals are depicted in Figure 7. Given a representative set-point profile, see the dashed curve in terms of scaled acceleration levels, three cases are

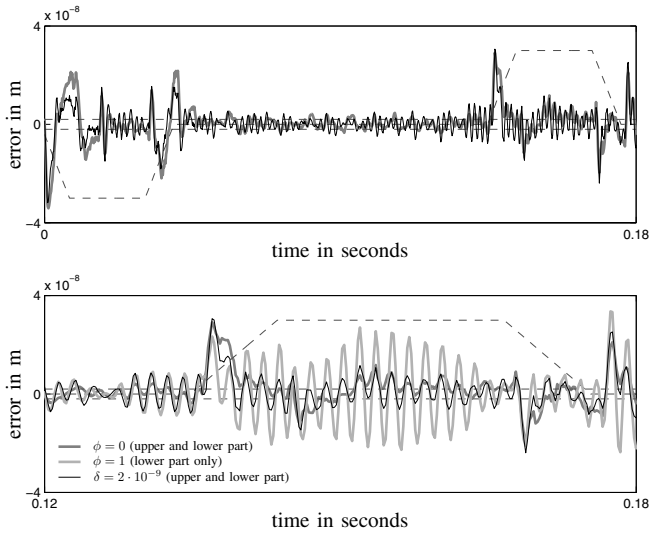

Fig. 7. Measured error time-series; upper part, linear low-gain feedback $\phi = 0$ versus nonlinear feedback $\delta = 2 \cdot 10^{-9}$, lower part, linear low- and high-gain feedback ($\phi = 0, \phi = 1$) versus nonlinear feedback $\delta = 2 \cdot 10^{-9}$.

considered: i) "low-gain" linear feedback with $\phi = 0$, ii) "high-gain" linear feedback with $\phi = 1$, and iii) nonlinear feedback with $\delta = 2 \cdot 10^{-9}$ (δ is tuned according to the error level at hand). By comparing the low-gain linear design with the nonlinear design, the upper part shows that neither feedback design seems particularly favorable from the (raw) error standpoint; the expected differences will become clear from a filtered perspective. Contrary the response under high-gain linear feedback, such as depicted in the lower part, demonstrates the negative effect of having too small stability margins under large excitation levels. Hence a large sensitivity to high-frequent oscillations resulting in a fairly large high-frequency response can be observed.

To quantify time response improvement, a so-called moving average filtered signal representation is used. In the semiconductor industry, moving average filtering expresses the means to reproduce details of the desired image. Based on the error sequence e, which is dictated by the sampling frequency $\mathrm{f_s}$, the moving average sequence is defined as

$$\mathcal{M}_a(i) = \frac{1}{n} \sum_{j=i-n/2}^{i+n/2-1} e\,(j),\ \forall i \in \mathbb{Z}, \tag{23}$$

with $n \in \mathbb{N}^+$ an application specific time frame. This operation acts as a low-pass filter operation on e, the result of which is depicted in Figure 8. In the indicated (grey) performance area, the infinity norm $\|\mathcal{M}_a(i)\|_\infty$ drops from 10^{-9} m to $3.2 \cdot 10^{-10}$ m, a ratio of improvement of 3.1 – the maximum ratio would be $1 + \alpha = 3.5$, see Figure 5.

In addition to moving average, the moving standard deviation is used to quantify the high-frequent parts in the time response. It expresses the fading properties of the created

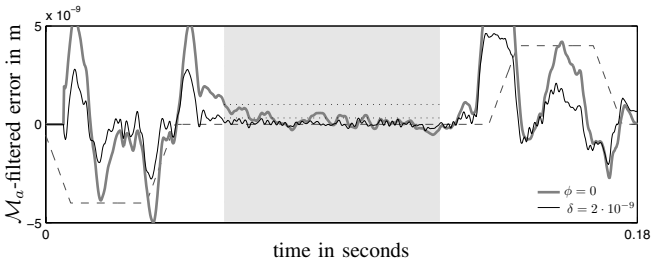

Fig. 8. $\mathcal{M}_a$-filtered time-series; linear feedback (ϕ = 0) versus nonlinear feedback ($\delta = 2 \cdot 10^{-9}$ m) within the indicated performance area.

image. The corresponding sequence is given by

$$\mathcal{M}_{sd}(i) = \sqrt{\frac{1}{n} \sum_{j=i-n/2}^{i+n/2-1} \left(e\,(j) - \mathcal{M}_a(i)\right)^2},\ \forall i \in \mathbb{Z}. \tag{24}$$

The result of this filter operation is depicted in Figure 9,

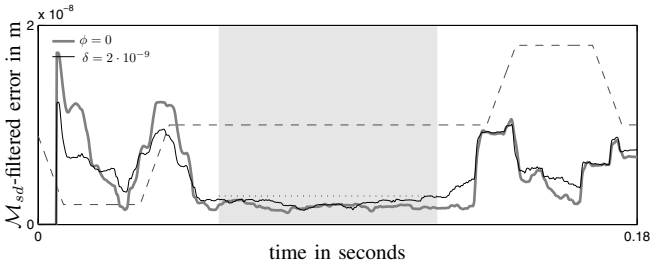

Fig. 9. $\mathcal{M}_{sd}$-filtered time-series; linear feedback ($\phi = 0$) versus nonlinear feedback ($\delta = 2 \cdot 10^{-9}$ m) within the indicated performance area.

where it can be seen that the infinity norm $\|\mathcal{M}_{sd}(i)\|_\infty$ in the indicated (grey) performance area only shows a marginal deterioration from $2.5 \cdot 10^{-9}$ to $2.9 \cdot 10^{-9}$ m.

E. Variable gains and stability margins

In terms of variable gains, Figure 10 shows the measured variability of the nonlinear controller gain along the considered error profile ($\delta = 2 \cdot 10^{-9}$). It follows that on average

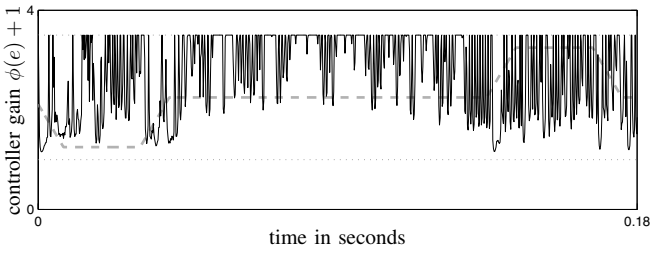

Fig. 10. Time-series of variable controller gains $\phi(e) + 1$ ($\delta = 2 \cdot 10^{-9}$ m) along the indicated (dashed) set-point profile.

the gain is large during the regions where the reference acceleration level is zero and small otherwise. Additionally, Figure 11 shows both phase- and gain-margin variations. With respect to the linear limit values (the dotted lines) it can

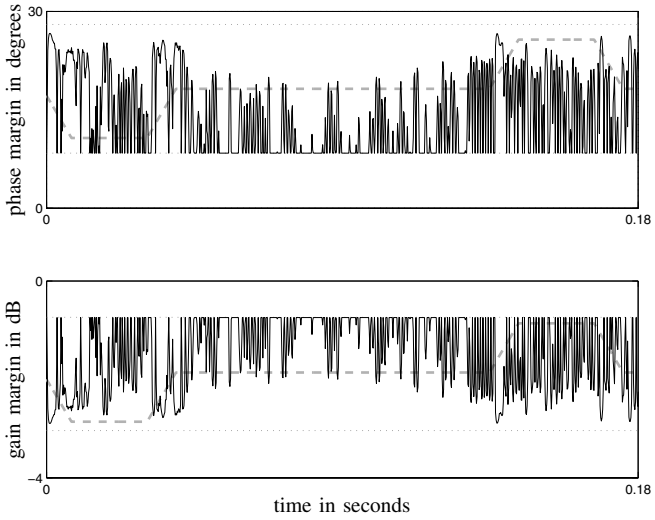

Fig. 11. Time-series of variable stability margins ($\delta = 2 \cdot 10^{-9}$ m) along the indicated (dashed) set-point profile.

be seen that the nonlinear feedback balances stability margins during the error profile in order to achieve performance.

F. Frequency-domain performance

In the frequency-domain, the benefit of nonlinear control is shown in Figure 12. By comparison of two nonlinear with two linear feedback realizations, it can be seen in

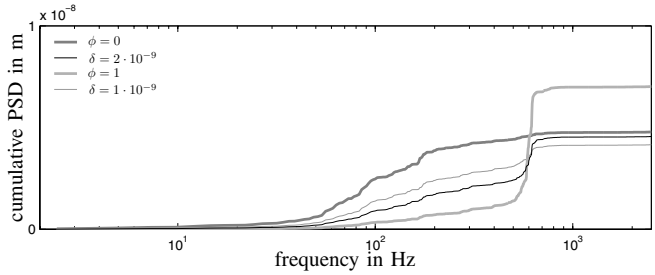

Fig. 12. Cumulative power spectral densities (PSD); linear feedback ($\phi = 0$ and $\phi = 1$) versus nonlinear feedback ($\delta = 1 \cdot 10^{-9}$ and $\delta = 2 \cdot 10^{-9}$ m).

terms of cumulative power spectral densities of the error signals that the high-gain linear design induces decreased low-frequency signal contents in comparison with the low-gain linear design. This comes at the cost of increased high-frequency signal contents. For the two nonlinear settings $\delta = 1 \cdot 10^{-9}$ and $\delta = 2 \cdot 10^{-9}$, it follows that the final values – the rms-values of the corresponding error signals – of both nonlinear controlled error signals are smaller than the corresponding values of both linear designs.

VI. Conclusions

For motion systems of a generally linear nature, a variable control design is proposed as a means to surpass linear design trade-offs. On the basis of a state-dependent nonlinear gain element, a nonlinear PID-based design is demonstrated to achieve performance by balancing stability margins over low-frequency disturbance rejection properties. Stability is addressed for a class of nonlinear PID-based controllers whereas design rules are considered for control design within this class. On the basis of measurements on an industrial wafer scanner, it is shown that the nonlinear design induces smaller error levels in terms of moving average (up to a factor of 3.1 improvement is demonstrated) without inducing significant deterioration of the error levels in terms of moving standard deviation. Besides, the rms-values of the error signals under nonlinear control become smaller than the corresponding values obtained with the linear control limits.

References

[1] Armstrong B, Neevel D, and Kusid T. (2001) New results in NPID control: tracking, integral control, friction compensation and experimental results. IEEE Transactions on Control Systems Technology, 9(2):399-406.

[2] Armstrong BSR, Gutierrez JA, Wade BA, and Joseph R. (2006) Stability of phase-based gain modulation with designer-chosen switch functions. International Journal of Robotics Research, 25:781-796.

[3] Freudenberg J, Middleton R, and Stefanopoulou A. (2000) A survey of inherent design limitations. In Proceedings of the American Control Conference, Chicago, Illinois: 2987-3001.

[4] Freudenberg JS, Hollot CV, Middleton RH, and Toochinda V. (2003) Fundamental design limitations of the general control configuration. IEEE Transactions on Automatic Control, 48(8): 1355-1370.

[5] Fromion V, Safonov MG, and Scorletti G. (2003) Necessary and sufficient conditions for Lur'e system incremental stability. In Proceedings of the European Control Conference, Cambridge, UK.

[6] Haddad WM, and Bernstein DS. (1991) Explicit construction of quadratic Lyapunov functions for the small gain, positivity, circle, and Popov theorems and their application to robust stability. In Proceedings of the Conference on Decision and Control, Brighton, UK: 2618-2623.

[7] Heertjes MF, Cremers FLM, Rieck M, and Steinbuch M. (2005) Nonlinear control of optical storage drives with improved shock performance. Control Engineering Practice, 13:1295-1305.

[8] Heertjes MF, Pastink E, Van de Wouw N, and Nijmeijer H. (2006) Experimental frequency-domain analysis of nonlinear controlled optical storage drives. IEEE Transactions on Control Systems Technology, 14(3):389-397.

[9] Leonov GA, Ponomarenko DV, and Smirnova VB. (1996) Frequency-domain methods for nonlinear analysis - theory and applications. World Scientific, Singapore.

[10] Lurie AI, and Postnikov VN. (1944) On the theory of stability of control systems. Journal of Applied Mathematics and Mechanics, 8(3):246-248.

[11] Minorsky N. (1922) Directional stability of automatic steered bodies. Journal of the American Society of Naval Engineers, 34(2): 280-309.

[12] Mulkens J, Streefkerk B, Hoogendorp M, Moerman R, Leenders M, De Jong F, Stavenga M and Boom H. (2005) Immersion lithography exposure systems: today's capabilities and tommorrow's expectations. SPIE, San Jose, California: 243-253.

[13] Rantzer A. (1996) On the Kalman-Yakubovich-Popov lemma. Systems & Control Letters, 28:7-10.

[14] Yakubovich VA. (1964) The matrix inequality method in the theory of the stability of nonlinear control systems - i. the absolute stability of forced vibrations. Automation and Remote Control, 7:905-917.

[15] Yakubovich VA, Leonov GA, and Ghelig AKh. (2004) Stability of stationary sets in control systems with discontinuous nonlinearities. World Scientific, Singapore.